Study of translaminar fracture toughness of unidirectional flax/epoxy composite

Yousef Saadati, Gilbert Lebrun, Christophe Bouvet, Jean-François Chatelain, Yves Beauchamp

Study of translaminar fracture toughness of unidirectional flax/epoxy composite

Yousef Saadati [a,*], Gilbert Lebrun [b], Christophe Bouvet [c], Jean-François Chatelain [a,*], Yves Beauchamp [d]

[a] Mechanical Engineering Department, École de Technologie Supérieure, 1100 Notre-Dame West, Montreal, QC H3C 1K3, Canada
[b] Mechanical Engineering Department, Université du Québec à Trois-Rivières (UQTR), 3351 boul. des Forges, Trois-Rivières, QC G9A 5H7, Canada
[c] University of Toulouse; INSA, UPS, Mines Albi, ISAE-SUPAERO, ICA (Institut Clément Ader), 3, rue Caroline Aigle, 31400 Toulouse, France
[d] McGill University, 845 Sherbrooke Street West, Montreal, QC H3A 0G4, Canada

Keywords:
Flax fiber
Translaminar fracture energy
Fracture toughness
Flax-epoxy composites
Tensile and compressive translaminar fracture
Infrared thermography

A B S T R A C T

Ever growing applications of flax fiber-reinforced composites (FFRCs) and their suitability for structural uses involve implementing the design and failure criteria for these composites. Translaminar fracture is one of the primary failure modes of unidirectional (UD) fiber-reinforced composites, and measuring it is essential for design purposes and in many material failure studies. However, the translaminar fracture parameters have not been evaluated for UD-FFRCs; thus, there is no data available in the literature. Moreover, conventional test methods for this failure mode are complex, and there is no standard method for measuring this value in compression. In this study, the translaminar fracture behavior of a UD flax/epoxy composite has been examined, and its fracture toughness in tension and compression in the fiber direction are determined following existing standard methods as well as using a methodology developed using infrared thermography. Compact tension specimens were adapted and used for this purpose. A fractographic study is conducted to examine the fracture surfaces and better understand the failure mechanisms. For tensile tests, the results of infrared thermography are in good agreement with those of ASTM E1922 and lie in the range of values obtained for similar composites in the literature.

1. Introduction

Over the last two decades, the need for materials with enhanced properties, lower cost, and improved sustainability has rendered natural (cellulosic) fiber-reinforced polymer composites (NFRPCs) an attractive alternative to their synthetic glass fiber (GFRP) counterpart in structural and non-structural applications [1–4]. Among natural plant fibers (NFs), flax is considered one of the most promising for polymer composites due to its unique properties [4–6]. Using continuous unidirectional (UD) and optimally configured reinforcements in NFRPCs is crucial to maximizing their load-carrying performance [7–9]. Therefore, UD flax fiber-reinforced composites (FFRPCs) are of prominent importance for the industry. In addition to strength and stiffness, fracture toughness is an essential property of fiber-reinforced polymer composites (FRPCs) for most engineering applications [10–12]. Nowadays, the engineering desire for an optimized, efficient, sustainable, cost-effective, and damage tolerant product design in conjunction with the ever-growing applications of FFRPCs necessitate characterizing the fracture toughness of these composites. The fracture toughness associated with translaminar failure mode (denoted by G_{IC}, when expressed in terms of energy and by K_{IC} when expressed in terms of stress intensity factor) is one of the primary mechanical properties of the fiber-reinforced composites (FRCs). This is particularly true when using the finite element method (FEM) to simulate specific material damages occurring in composite laminates, like fiber failure, matrix breaking, and delamination [13–17]. The FEM approach requires different fracture energies as input variables, and the fracture toughness in different directions and their corresponding evaluation methods are prerequisites for the FEM simulation of FFRPCs. While the significance of translaminar fracture toughness (TFT) measurement was recognized since the late '70s, it has attracted little interest [18]. This is because FRCs were not used in primary structures, where this property is mostly required. At the same time, the advanced numerical simulation methods referring to this property were not yet developed [18]. The situation is now different as FRCs are used in structures, and FEM is a commonly used numerical method. With the growing application of NFRPCs, their TFT is expected to play an essential role in the

* Corresponding authors.
E-mail addresses: yousef.saadati.1@ens.etsmtl.ca, yousef.saadati.1@gmail.com (Y. Saadati), gilbert.lebrun@uqtr.ca (G. Lebrun), christophe.bouvet@isae.fr (C. Bouvet), jean-francois.chatelain@etsmtl.ca (J.-F. Chatelain), yves.beauchamp@mcgill.ca (Y. Beauchamp).

https://doi.org/10.1016/j.jcomc.2020.100008

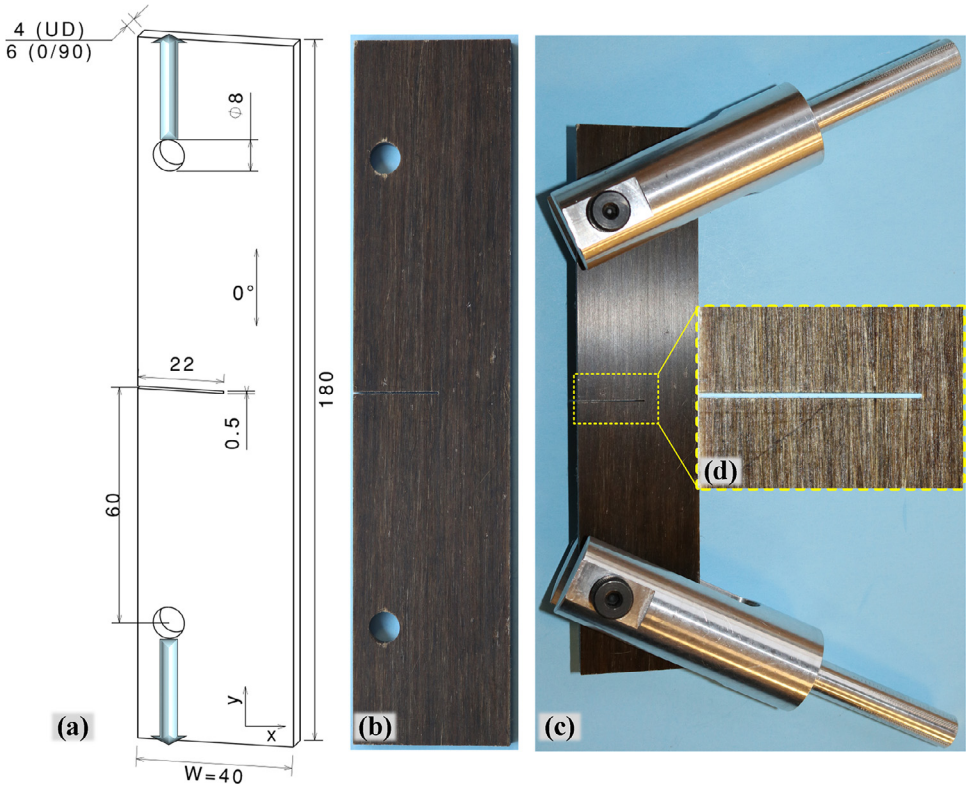

Fig. 1. The ECT configuration (a), test specimen (b), load application configuration (c), and notch (d). (Dimensions in mm).

future. Currently, it is required in many research fields, such as the machining of composite materials, where numerical models based on FEM are involving.

In the literature, measuring the translaminar fracture toughness of NFRPCs is limited to a few studies that are all conducted only in tension. Hughes et al. [11] studied the TFT of some chopped NFRPCs and compared them to that of a glass fiber mat composite. The G_{IC} value of GFRP was three-fold higher than those of NFRPCs. They concluded that different micro-structural toughening mechanisms were activated in the NFRPCs compared to GFRP. Silva et al. [19] reported an in tension G_{IC} = 11.8 kJ/m^2 for woven sisal/polyurethane (PU) composite. They observed that G_{IC} increased with fiber volume fraction (V_f) and was impaired with the alkaline treatment of the fibers. Liu and Hughes [12] investigated the effects of textile yarn linear density, weave configuration, and stacking sequence on G_{IC} of woven FFRECs. They measured the K_{IC} of anisotropic woven-flax/epoxy composites following BS 7448 standard. According to their findings, the fracture behavior and K_{IC} are strongly dependent on the linear density of yarns and the direction of the test but is independent of the weave type. The authors reported K_{IC} values in the range of 3–8.5 MPa m$^{1/2}$ for the composites and concluded that the fracture toughness is more dominated by the fiber properties and V_f rather than the reinforcement configuration. Following ASTM D5045, Li et al. [20] studied the fiber surface treatment effect on fracture properties of textile-sisal/vinyl-ester composite. They obtained K_{IC} = 4.2 MPa m$^{1/2}$ for the untreated fiber composite, which increased to 5.5 and 6.0 MPa m$^{1/2}$, respectively, with Silane and $KMnO_4$ fiber treatments. Ismail et al. [21] reported values of $K_{IC} \approx 8.5$ and $K_{IC} \approx 4.5$ MPa m$^{1/2}$, respectively for UD-twisted yarn and cross-ply woven kenaf/polyester composites tested based on ASTM D5045. Chizyuka and Kanyanga [22] investigated the effects of hydrothermal aging and moisture absorption on the K_{IC} of sisal/polyester composites. They followed the ASTM E1922 procedure to evaluate the K_{IC} of the composites and obtained $K_{IC} \approx 6.25$ MPa m$^{1/2}$. The fractographic study revealed that the reduction of K_{IC} after moisture absorption was mainly due to fiber/matrix debonding, which was the dominant fracture mechanism in the composite. Manjunath et al. [23] followed ASTM E1922 and investigated the K_{IC} of jute fabric reinforced epoxy composites. However, the criteria of the standard were not carefully respected, and there is a mismatch between their reported test data and the reported K_{IC} values. Their result is also one order of magnitude higher than that of Ashik et al. [24], K_{IC} = 7.71 MPa m$^{1/2}$, for an analogous material.

1.1. Translaminar fracture toughness in tension

The ASTM E1922 standard [25] suggests the extended compact tension (ECT) specimen for measuring the tensile TFT of FRCs. ECT, Fig. 1, is an extended configuration of the compact tension (CT) specimen, Fig. 2(a), which was developed to overcome undesirable failure modes such as crack growth perpendicular to the pre-notch [26,27]. ASTM E1922 was developed and adapted to measure the fracture toughness of FRCs in tension, while a number of studies have used CT specimens, along with ASTM E399, D5045, or other methods [28–33]. Without mentioning any particular reason, several researchers tested cross-ply laminates and utilized a rule-of-mixtures type approach to measure the fracture toughness of UD-FRCs [18]. Jose et al. [17] evaluated the tensile TFT of a carbon/epoxy cross-ply laminate $[0/90]_{15}$ as well as its constituent UD laminates, $[0]_{30}$ and $[90]_{30}$. They presented an analytical relationship between the K_{IC} of the laminate and those of its constituent UD sub-laminates. However, some of their specimens failed improperly, and their derived equation seems to have inconsistent dimensions. Pinho et al. [28] used a similar approach to determine the G_{IC} associated with the tensile and compressive failure of UD carbon/epoxy laminates using a cross-ply $[0/90]_{8S}$ laminate. They used CT and CC specimens with the dimensions and fiber direction shown respectively in Fig. 2(a) and (b) and followed the ASTM E399 procedure. However, they regenerated a finite-width correction factor based on FEM to replace the one defined in ASTM E399 for isotropic materials. The authors assumed: (i) that the mode-I critical energy release rate of the cross-ply laminate is the sum of energies associated with the fiber fracture in the 0° layers and matrix

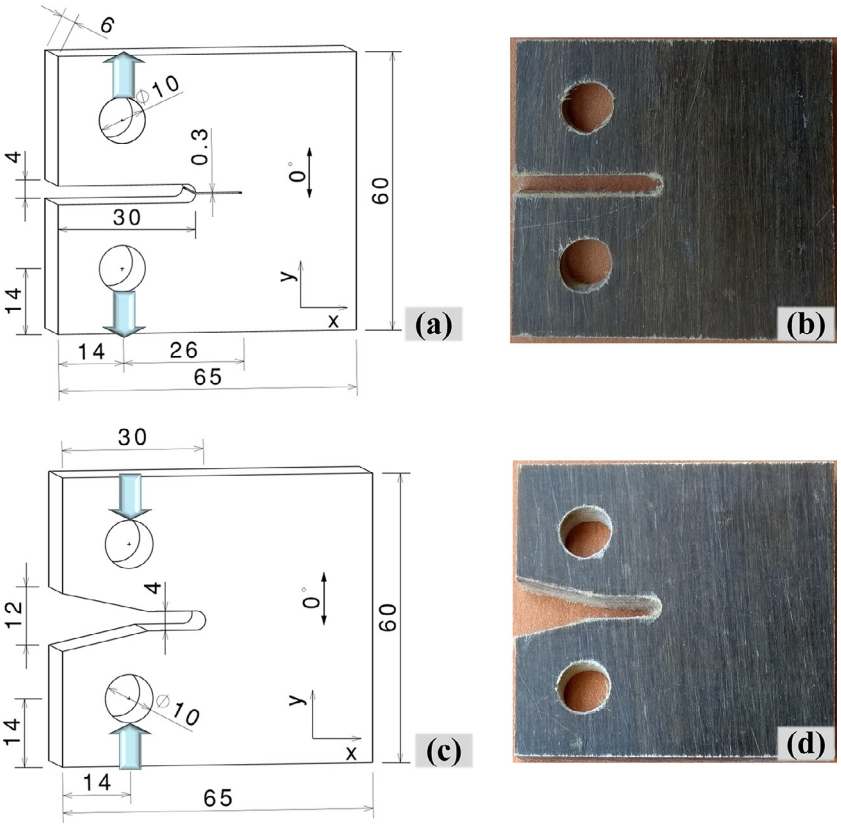

Fig. 2. The CT (a) and CC (c) configurations and CT (b) and CC (d) test specimens (Dimensions in mm).

cracking in the 90° layers (they thus neglected other damage modes and interaction between neighboring layers) and (ii) that the matrix cracking in the 90° layers occurred as a single crack parallel to the notch (similar to delamination mode-I). With this last assumption, the critical energy release rate in tension is quantitatively equivalent to that of mode-I delamination. This assumption seems reasonable, as the 0° layers are much tougher than the 90° layers, and is found to be a good approximation based on their findings in a previous work [34]. For the particular cross-ply lay-up studied, they derived an equation used to calculate the G_{IC} for the UD laminate. Later on, Laffan et al. [32] used the following generalized form of the derived equation (with the same assumptions) to study the lay-up effects on the fracture toughness of carbon/epoxy composites in tensile fiber failure mode;

$$G_{IC}^{0} = \frac{t_{lam}}{t_0} G_{IC}^{lam} - \frac{t_{90}}{t_0} G_{IC}^{90} \tag{1}$$

where t_{lam}, t_0 and t_{90} are the thicknesses of the laminate, 0° and 90° layers within the laminate, respectively. G_{IC}^{0} is the fracture energy associated with the fiber tensile failure mode, and G_{IC}^{90} represents the intralaminar mode-I matrix cracking fracture energy. In another study, Laffan et al. [35] observed that there was no interaction between the failure modes occurring in the 0° and 90° plies. This result confirms their approach. Nevertheless, it has been shown that the lay-up in the cross-ply laminates can affect the G_{IC} measured for the 0° plies [18,32,36,37]. Donadon et al. [38] followed the same approach to calculate the fracture energy in woven cross-ply laminates along with a numerical method. The agreement of the experimental and numerical results confirmed the validity of this approach.

1.2. Translaminar fracture toughness in compression

By contrast to TFT in tension, there is no standard test method available to evaluate the fracture toughness of FRCs in compression. In a few works [28,30], modified CT specimens are used in compression with the test coupon renamed compact compression (CC). Pinho et al. [28] used the same approach explained in the previous section for determining TFT in compression of UD laminates. They used CC specimens with the configuration shown in Fig. 2(c) and (d) and followed the ASTM E399 procedure. They made the same assumptions considering that in compression loading, the matrix cracking in the 90° layers is close to what happens in delamination mode-II. Thus, the critical energy release rate in compression is quantitatively equivalent to that of mode-II delamination. They used Eq. (2) to calculate the G_{IC} for the UD laminate in the fiber direction;

$$G_{IC}|_{fiber\ kinking} = 2G_{IC}|_{lam\ comp} - G_{IIC}|_{matrix\ intra} \tag{2}$$

where $G_{IC}|_{lam\ comp}$ is the critical energy release rate of the laminate, as measured by a CC test, $G_{IIC}|_{matrix\ intra}$ is the mode-II matrix failure intralaminar fracture energy, and $G_{IC}|_{fiber\ kinking}$ is the fracture energy associated with fiber-kinking failure mode. Overall, there is a significant difference between the fracture toughness values reported by the authors using different approaches to measure compressive TFT [18,33]. Perhaps this indicates that conventional mechanical tests are not suitable for this purpose. The compressive fiber failure mode in laminated composites is known as a very complex phenomenon, which is the result of fibers micro-buckling and formation of kink-bands or crushing [28,39,40]. So, and unlike tension, the authors observed large damage zones. Therefore, to measure the pure TFT in compression, the damage mechanisms should be separated.

1.3. Infrared thermography/Translaminar fracture toughness measurement

In the past two decades, infrared thermography (IRT) has been broadly used to investigate the energy-dissipative processes in materials, for example, plastic deformation in metals [41] or damage in polymeric materials [42]. For composite materials, Naderi et al. [43] used IRT to characterize the damage evolution in fatigue loading. They found that the results were consistent with those obtained by acoustic emis-

Table 1
Configuration and applications of flax/epoxy laminates

Plate	Application Test	Specimen type	Layup	Fiber surface density (g/m^2)	Volume fraction (%)	Thickness (mm)
1	E1922	ECT	$[0]_{12}$	200	41	4.04
2	IRT	CT and CC	$[(0/90)_4/0]_s$	200	41	6.06
3	E1922	ECT	$[(90/0)_4/90]_s$	200	41	6.06

sion, while Lisle et al. [44,45] used it to study damage development in fabric-glass/epoxy composites. The relation between fracture toughness and dissipative work has already been proved [46], and depending on the material, the ratio of the dissipative work converted into thermal energy can vary between 10 and 100% [47,48]. Lisle et al. [49] showed that for a carbon/epoxy composite, the ratio of dissipative work converted to heat should be close to 100%, but for metallic materials, this ratio is usually lower. The authors used the IRT to measure the fracture toughness of the GFRP in tension [45] and that of the UD-carbon fiber-reinforced polymer (CFRP) composite in compression [49,50]. IRT made it possible to separately assess the dissipated energy due to fiber failure in compression and eliminate those associated with material crushing at loading points or secondary cracks. They obtained a value of G_{IC} = 42.5 N/mm in compression and found their results consistent with those of Hongkarnjanakul et al. [51] (40 N/mm) and other researchers [28,39]. There is no previous research using this approach to address NFRPCs.

In summary, no standard test methods have been developed for measuring G_{IC} of NFRPCs and of FRCs in compression, and a very limited number of studies have addressed these topics, while all NFRPCs have been tested in tension. These are essential properties for engineering design purposes and the modeling of these materials with numerical methods, such as FEM. Moreover and to our knowledge, no fractographic and micrographic analysis of this subject have been performed for UD-flax fiber-reinforced epoxy composites (FFRECs). The work presented in this study aims at evaluating the fracture energy associated with the translaminar failure of the UD-FFRECs, using two methodologies, along with an investigation of the fracture behavior and viability of the standard test procedures for FFRECs considering that these procedures are used for synthetic (glass or carbon) FRCs. In the first method, the composite was tested according to the existing ASTM E1922 standard. The translaminar fracture was studied, and the G_{IC} value in tension for crack propagating perpendicular to fibers was determined and validated. In the second method, employing the IRT-based methodology developed and implemented for this purpose by Lisle et al. [45,49,50] as well as ASTM D5045 standard, G_{IC} of UD-FFRECs in tension and compression was determined, and the material behavior was assessed.

2. Material system and test specimens

Unidirectional flax fibers, FLAXTAPE^{TM} 200 (from LINEO – France), with a width of 400 mm and surface density of 200 g/m^2, were used to reinforce Marine 820 Epoxy System, mixed with 18 wt% Marine 824 hardener (from ADTECH® Plastic Systems), to prepare the UD-FFREC laminates. The composite laminates were molded using the RTM process. The layers of flax fibers were stacked up according to the required number of layers and orientation of fibers. 300 mm × 300 mm composite plates were molded, starting with $[0]_{12}$ and $[(0/90)_4/0]_s$ laminates, respectively for ECT and CT/CC specimens; then, a third configuration, $[(90/0)_4/90]_s$, has been used to improve the translaminar crack propagation for ECT specimens, as detailed in Table 1.

The number of layers and thickness of laminates were precisely calculated, according to the ASTM D3171 procedure, and controlled with spacers during molding to result in a constant V_f = 41% for all composite plates while attaining the required thickness for the test specimens.

ECT specimens were prepared according to ASTM E1922 for evaluating the TFT in tension. Fig. 1 shows the configuration and photograph of a typical specimen. The CT and CC specimens used for TFT measurement in combination with IRT were prepared according to in-plane dimensions specified in Pinho et al. study [28]. The configurations and photographs of typical specimens are shown in Fig. 2. The same type of CT specimen was also used in [31,32,35]. Pujols Gonzalez et al. [52] used CT and CC specimens to evaluate in tension and compression TFT of CFRP composites using IRT-based methodology, respectively. A similar methodology is adapted and employed in this study. Rectangular specimens were cut by a 10-inch/90-tooth, DIABLO's cutting saw blade, with high-density carbide tooltips. Then, the loading-pin holes were drilled with the help of sacrificed plates to avoid damages to the specimens. A Protostar® mini corner radius solid carbide shoulder/slot milling cutter (Protostar®-Walter tools) was used to cut the notch in ECT specimens. As can be seen in Fig. 1(d), despite the low machinability of NFRPCs in terms of surface quality, a very neat notch is cut without damaging the composite. The 4 mm-notch on the CT and CC specimens were cut using a milling cutter; the notch mouth on the CC was widened, and the final notch (pre-crack) on CT was cut using a wire saw. Two clevises were also designed and manufactured to eccentrically introduce the load to the specimens (Fig. 1(c)).

3. Translaminar fracture tests and data reduction methods

3.1. Standard tension testing of ECT specimens

ASTM E1922 standard involves tension testing of single-edge-notch specimens to determine the tensile TFT of various carbon and glass/polymer composites. However, it can be applied to other FRPCs, provided that the specimen dimensions and the test results satisfy the requirements of the standard [25]. Following the guidelines of this standard and aiming at measuring the fracture toughness of the UD-FFRECs in the current study, ECT specimens (Fig. 1(b)) were cut from the UD-FFREC laminate with a nominal thickness of 4 mm (plate 1 in Table 1). Here, the low stiffness of the ECT specimens made it impossible to install the conventional extensometers, using knife edges, at the notch-mouth to measure the notch mouth opening displacement (NMOD). Alternatively, a digital image correlation (DIC) setup, synchronized with load application, was used for this purpose, as shown in Fig. 3(a). However, none of the five ECT specimens tested with such setup experienced a self-similar (parallel to the pre-notch) crack growth and did not result in effective translaminar crack growth of concern in this test method. Indeed, the crack propagated perpendicular to the notch and in the fiber direction, which invalidated the tests, as shown in Fig. 3(b). To the authors' knowledge, no ECT specimens of synthetic or natural UD-FRCs have been tested in the literature, the reported ECT tests are mostly for natural/synthetic fabric or cross-ply reinforcement architectures [18,22,23,53], and a few were from pultruded composites [14]; therefore, no benchmark study was possible, and these experiments were unavoidable.

To overcome this difficulty, cross-ply laminates were used to avoid the large difference in strength between the longitudinal and transverse direction of the test specimen, such that each 0° layer is backed by a 90° layer to inhibit crack propagation perpendicular to the notch, similar to the approach in [28,32]. Eq. (1) is used to calculate the translaminar fracture energy of UD plies using that of a cross-ply laminate and the Mode I and Mode II interlaminar fracture energies of the UD laminate. For this purpose, a second laminate was fabricated (plate 3 with the lamination sequence of $[(90/0)_4/90]_s$ and nominal thickness of 6 mm),

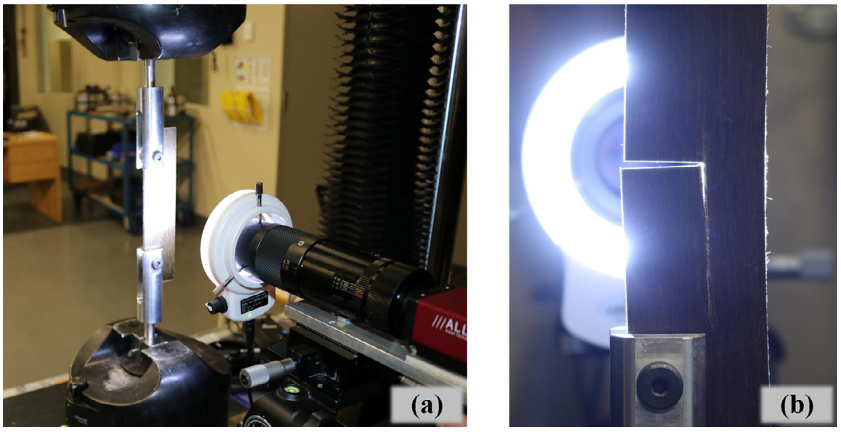

Fig. 3. Test setup with DIC used to measure NMOD (a) and failed ECT UD specimen (b).

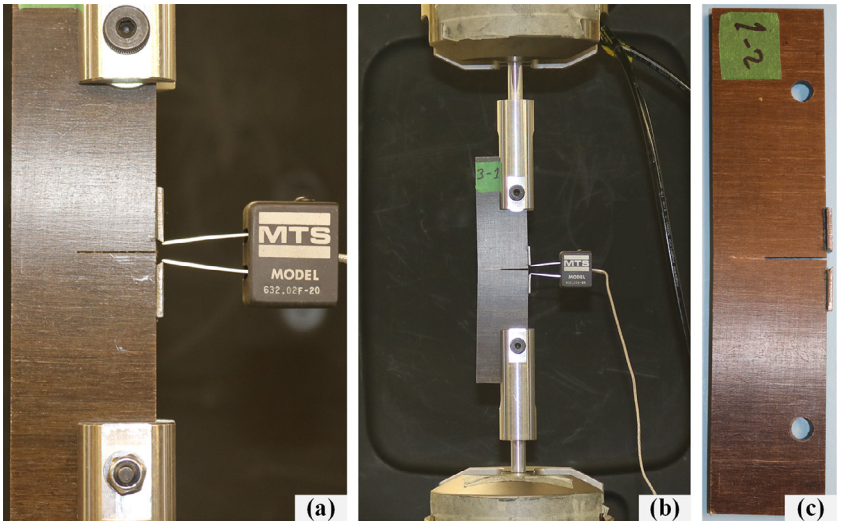

Fig. 4. ECT specimen; knife edges and installed extensometer (a) test setup (b), and failed sample (c).

and ECT specimens (Fig. 1(a)) were cut and prepared. These thick and stiff enough specimens made possible the installation of an extensometer to measure the mouth opening. Therefore, precisely machined knife edges were bonded to the specimens' edge on both sides of the notch mouth, Fig. 4, and the extensometer MTS (632.02F-20) was installed to measure the notch-mouth-opening displacement (NMOD). The tests were conducted with a 0.7 mm/min crosshead displacement rate on an MTS (858 Mini Bionix-II) machine, with a mounted 15 kN load-cell. The test setup and specimen are shown in Fig. 4(a) and (b). The tests continued until the applied force dropped to a magnitude of less than 50% of the peak load. The specimen exhibited a translaminar self-similar crack growth, as expected, Fig. 4(c).

Data reduction was performed according to ASTM E1922, and the TFT was calculated through the stress intensity factor approach, as;

$$K_{Ic} = \left[\frac{P_{max}}{BW^{1/2}}\right] \frac{\alpha^{1/2}[1.4+\alpha]\left[3.97 - 10.88\alpha + 26.25\alpha^2 - 38.9\alpha^3 + 30.15\alpha^4 - 9.27\alpha^5\right]}{[1-\alpha]^{3/2}} \quad (3)$$

where K_{Ic} is the critical stress intensity factor (MPa $m^{1/2}$), P_{max} is the maximum applied or fracture load (MN), $\alpha = a/W$ is a dimensionless parameter, while a is the notch length, B is specimen thickness, and W is specimen width (a, B and W are in meter). According to the standard, K_{Ic} provides a valid measure of TFT, when the damage zone is relatively small. This criterion is defined based on NMOD values at maximum load as $\Delta V_n/V_{n-0} \leq 0.3$, for ΔV_n and V_{n-0} shown in Fig. 6. For orthotropic plates under plane stress (with a pre-crack subjected to in-plane loading), the fracture energy G_{IC} can be calculated from K_{Ic} as

Table 2
Mechanical and thermal properties of UD-FFREC ply [56]

Longitudinal elastic modulus, E_{11}	22.69* GPa
Transverse elastic modulus,E_{22}	4.34* GPa
Shear modulus, G_{12}	1.92 GPa
Poisson's ratio, υ_{12}	0.4*
Density, ρ	1280 kg/m^3
Specific heat, C	665 J/kg/K
Thermal conductivity in normal (z) direction, k_{33}	0.115 W/m/K

* Average of the values in tension and compression.

Table 3
Elastic properties of $[(90/0)_4/90]_s$ laminate

E_{xx} (GPa)	E_{yy} (GPa)	G_{xy} (GPa)	υ_{xy}
14.74	12.68	1.92	0.14

follow [17,28,39,54,55]

$$G_{Ic}^{lam} = \frac{K_{Ic}^2}{\sqrt{2E_{xx}E_{yy}}}\left[\left(\frac{E_{xx}}{E_{yy}}\right)^{1/2} + \frac{E_{xx}}{2G_{xy}} - \upsilon_{xy}\right]^{1/2} \quad (4)$$

where E_{xx}, E_{yy} are the laminate elastic moduli respectively in the x and y directions (shown in Figs. 1(a), 2(a), and (c)), G_{xy} is the laminate shear modulus, and υ_{xy} is the Poisson's ratio. For the $[(90/0)_4/90]_s$ laminate, these properties, presented in Table 3, are calculated from those of the UD laminate given in Table 2, published in a previous work [56], by using the classical laminate theory [57].

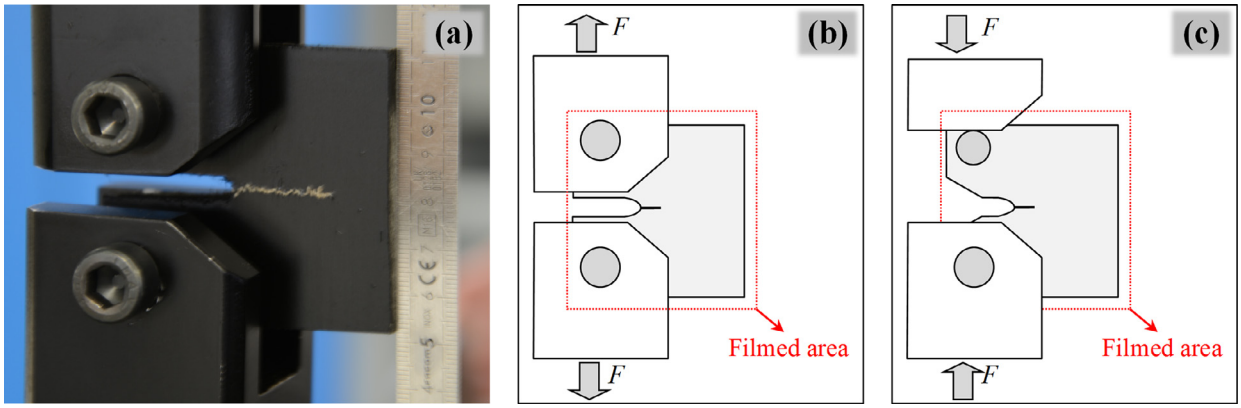

Fig. 5. Experimental setup for IRT methodology (a), test specimen and thermal investigation area for CT (b) and CC (c).

3.2. Infrared thermography method

In order to overcome the problems experienced with experimental methods used to study the translaminar fracture of composite materials, it was proposed to develop an approach allowing estimating the rate of energy release via the temperature measurement in [43,45,49,50]. Characterizing the fracture energy utilizing IRT is an idea conceptualized based on the principles of irreversible thermodynamics and thermomechanical laws. The complete details of the methodology, including all assumptions made and their validity, are well described in 45,49,50] for evaluating the tensile and compressive fracture energy of FRCs, and the reader should refer to these documents for more details.

Having the dissipated energy evaluated with IRT, the fracture energy,G_{IC}, can be determined using Eq. (5) [45,49].

$$G_{IC} = \frac{dW_{irrev}}{dA} = \frac{dW_{diss}}{\beta . dA} \tag{5}$$

where dW_{irrev} denotes the total irreversible energy, dW_{diss} is the energy dissipated as heat,$dA$is the crack surface growth and $\beta = \frac{dW_{diss}}{dW_{irrev}}$ is the Taylor–Quinney coefficient ($0 \leq \beta \leq 1$).

Some studies of metallic materials reported $\beta \approx 1$ for Ta [47,49] and $0.5 \leq \beta \leq 1$ for stainless steel, depending on the applied strain rate [49]. However, allocating value for this ratio remains a delicate issue in this study, because, no values are available for the flax/epoxy composite under study. Furthermore, the magnitude of the coefficient is strain and strain-rate dependent [45,48,49]. Li and Lambros [48] investigated PMMA and PC polymers in terms of the value of β and its sensitivity to strain and strain-rate. The authors found it impossible to measure β for PMMA; however, they reported values between 50% for high strain and 100% for low strain, independent of the strain-rate in the ranges of the investigation. Considering the available β values for polymers in the literature, values of $\beta = 0.5$ and $\beta = 0.9$ were chosen for this study. The results are then compared to those obtained from the ASTM E1922 standard test method to evaluate the validity of the assumptions.

In this study, the 3D thermal analysis methodology developed in [45,49] is utilized to evaluate the heat sources in the composite using the thermal properties in Table 2, from which the dissipated energy and then, using Eq. (5), the critical energy release rate or fracture energy G_{IC} is calculated. For this purpose, the adapted CT and CC specimens from [28], shown in Fig. 2, were cut from $[(0/90)_4/0]_s$ laminate (Plate 2 in Table 1) and mechanically loaded in tension and compression respectively. CT tests were conducted following ASTM D5045 standard, and CC tests were performed with the same procedure with a compression loading. The temperature change at the surface of the specimen (outermost 0°-ply of the $[(0/90)_4/0]_s$ laminate) was simultaneously recorded and synchronized with the load and displacement data. The test setup is shown in Fig. 5(a). It can be noticed that for the CC tests, the grip of the machine was only put on the axis of load introduction in order to have a larger filmed area (Fig. 5(c)). The translaminar fracture tests were carried out on an electromechanical traction machine (INSTRON 100kN) at ambient temperature (≈25°C) and a constant displacement rate of 2 mm/min. The thermal data of the specimen surface was recorded at a frequency of 50 Hz using an infrared camera (FLIR SC7000) with a resolution of 320 × 256 pixels, and a thermal resolution of 0.025 K for temperature variation measurement. The spatial resolution (pixel size) determined by the focal distance is set at 0.264 mm. The target surface of the specimen was painted black in order to maximize the emissivity coefficient, and then the value is supposed to equal 1 for data treatment. As expected, for CT specimens, the through-the-thickness crack propagated parallel to the 90° fibers by breaking the fibers in the 0° layers and created almost a planar fracture path, Fig. 5(a). The fracture path at the edge of the specimen opposite to the notched side shows that the crack path is almost planar.

4. Results and discussion

4.1. Standard tension testing of ECT specimens

A typical load vs. NMOD curve of a cross-ply ($[(90/0)_4/90]_s$) ECT specimen is shown in Fig. 6. From this curve, it can be observed that the composite exhibits a linear behavior (R^2=0.997) up to around 80% of the maximum load. Subsequently, upon initiating the damage zone ahead of the notch tip, a gradual deviation from linearity appears and continues up to the peak load. After reaching the peak value, the load decreases slowly with no sudden drops, meaning that a stable translaminar fracture occurs and propagates, consistent with the observations during the test. Similar behavior was observed for woven-flax/epoxy composites tested using CC specimens [12], woven-sisal/polyester composites tested using ECT [22], and woven-sisal/PU composites tested by CT specimens [19]. On a macroscopic scale, the wake of self-similar crack can be seen on a failed specimen in Fig. 4(c), satisfying the requirement of the ASTM E1922 concerning effective translaminar crack growth. As shown for the typical specimen in Fig. 6, the additional NMOD during fracture, ΔV_n, fulfills the criterion of ASTM E1922, in this case with $\Delta V_n/V_{n-0} = 0.18 \leq 0.3$, and validates the translaminar fracture toughness (K_{IC}) obtained using Eq. (3) for all the tests.

Substituting the α parameter value in Eq. (3) and using the maximum load, the K_{IC} of the cross-ply specimens ($[(90/0)_4/90]_s$) was computed, and the results are summarized in Table 4. The fracture energy (G_{IC}^{lam}) was subsequently obtained from the data in Table 3 and Eq. (4) and is also presented in Table 4. As discussed earlier, Eq. (1) is used to calculate the fracture energy of the 0° sub-laminates (G_{IC}^{0}) where G_{IC}^{90} is assumed to be equivalent in magnitude to the mode-I interlaminar fracture energy of the UD-FFREC, G_{IC}^{delam}, which was evaluated in a separate study as $G_{IC}^{delam} = 0.691$ kJ/m^2 [58]. Accordingly, t_0 and t_{90} were obtained by considering they are proportional to the number of the corresponding

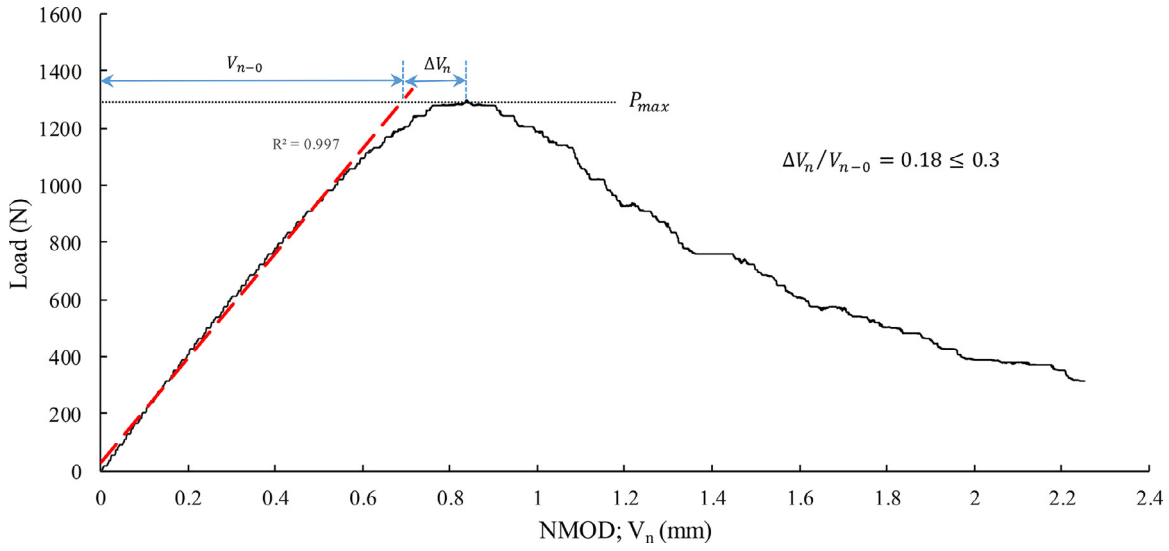

Fig. 6. Load vs. Notch-mouth-opening displacement (NMOD) curve.

Table 4
Fracture toughness and fracture energy of UD-FFREC

	K_{IC}^{lam} (MPa m$^{1/2}$)	G_{IC}^{lam} (kJ/m^2)	K_{IC}^{0} (MPa m$^{1/2}$)	G_{IC}^{0} (kJ/m^2)
Mean	8.07	7.37	14.27	15.71
STD	0.30	0.55	0.57	1.23
C.O.V. (%)	3.78	7.41	3.99	7.82

plies in the laminate, i.e., 8 and 10 plies. For comparison purposes with the literature data, K_{IC}^{0} of the UD-FFREC laminate was calculated back from G_{IC}^{0} and its elastic properties (given in Table 2) using Eq. (4). The results are presented in Table 4.

It is difficult to compare these results with the literature considering the very limited works published on the measurement of TFT in NFRPCs, particularly FFRECs. Nevertheless, the value obtained for K_{IC}^{lam} is in excellent agreement with the results published by Liu et al. [12] for woven-flax/epoxy CT tests, shown in Table 5. They published K_{IC}^{lam} values in the range of 3 to 8.5 MPa m$^{1/2}$, albeit at lower V_f (from 31% to 35%), that covers the obtained value in this study. The $K_{IC}^{lam} = 7.2$ MPa m$^{1/2}$ mentioned in Table 5, with the reinforcement configuration most consistent with the cross-ply laminate tested in this present study but for a fabric instead of UD reinforcement in the present study, should be compared to the value of K_{IC}^{lam} in Table 4. Overall, their results are consistent with the findings of the present study, considering the V_f and different ply architecture, and these two studies confirm each other. K_{IC} = 7.71 MPa m$^{1/2}$ reported by Ashik et al. [24] for 50/50 wt% woven-jute/epoxy composite (Table 5) is also in the range of the obtained results. The higher fiber content, but lower strength of jute fibers could have balanced the toughness to be consistent with the result of the present work [3,11,59]. Chizyuka and Kanyanga [22] obtained K_{IC} = 6.5 MPa m$^{1/2}$ for fabric-sisal/polyester composites with V_f between 50% to 55% (Table 5). The lower K_{IC} of this composite can be attributed to the lower tensile strength of sisal fibers compared to flax fibers [3,11,59]. On the other hand, Silva et al. [19] reported $G_{IC} \approx 11.5$ and $G_{IC} \approx 7$ kJ/m^2 respectively for a fabric and short fiber sisal/PU composite with $V_f \approx 0.30$ (Table 5). The G_{IC} of short fiber sisal/PU composite is in the range of our results, but that of sisal-fabric is much higher. Due to reporting the toughness of sisal-fabric/PU in the form of G_{IC}, it cannot be compared with those of similar materials; fabric-sisal/polyester composite reported in [22] and textile sisal/vinyl-ester reported in [20], both indicated by K_{IC}, see Table 5. The authors attributed the high performance of fabric-reinforced PU to the better compatibility between NFs and natural resins and to the structure of the reinforcement. Li et al. [20] reported a K_{IC} = 4.2 MPa m$^{1/2}$ for a textile sisal/vinyl ester composite at $V_f \approx 0.32$, which increased to 6 MPa m$^{1/2}$ after applying a fiber surface treatment. Hughes et al. [11] measured K_{IC} = 5.04 and K_{IC} = 5.62 MPa m$^{1/2}$ respectively for jute and hemp non-woven felt reinforced polyester, Table 5. The reported $K_{IC} \approx 8.5$ MPa m$^{1/2}$ by Ismail et al. [21] for UD twisted-kenaf-yarn/polyester composites is also consistent with the values determined in this research, Table 5. Considering the reasonable variability of the results and after comparing them to the available literature data, it can be concluded that the measured values are a realistic representation of the fracture toughness and fracture energy of the FFREC.

4.2. Fractography of the ECT specimens

The fracture paths of ECT specimens when the load dropped to about $0.2P_{max}$, are shown in Figs. 4(c) and 7(a). The failed specimen is not separated into two parts to expose the fracture surface, so it is difficult to examine the fracture in terms of failure mechanisms. On the other hand, separating the two parts of the specimen would alter the rupture faces. Nevertheless, to perform a microstructural study and explore the fracture mechanisms, one of the specimens was loaded up to full separation to expose the fracture surface near the notch tip.

The micrographs are shown in Fig. 7(a) and (b). At the surface ply, which is a 90° ply oriented parallel to the notch, matrix cracking and splitting of the ply has occurred, and then, with crack growth, fiber-matrix debonding and fiber bridging have developed. In addition, the crack emanated from the corner of the notch and propagated in a self-similar manner. For further analysis of the failure mechanisms, the fracture surface is investigated from three viewing directions, as indicated in Fig. 8(a). The normal view of the fracture surface, Fig. 8(b), clearly shows the 0° and 90° layers. Fiber-matrix debonding and matrix cracking can be observed in the 90° plies, while fiber fracture occurred in the 0° plies. The side view in Fig. 8(c) shows a huge fiber pull-out, fiber bundle fracture, and fiber bundle splintering. These phenomena are accepted as the dominant failure modes contributing to fracture toughness in composites [19,28,32,35]. The high volume of fiber pull-out is an indication of the poor fiber-matrix adhesion (due to poor compatibility of hydrophilic NFs towards the hydrophobic polymer matrix), resulting in weak interfaces that have been observed several works [11,20,56,60]. Although fiber pull-out is a mechanism that accounts for significant energy absorption in FRCs [11], poor fiber-matrix adhesion along with fiber slippage inside the flax bundle after fiber fracture could ease the

Table 5
Literature data for fracture toughness of NFRPCs

	K_{IC}^{lam} (MPa m$^{1/2}$)	K_{IC}^{lam} (MPa m$^{1/2}$)	K_{IC}^{lam} (MPa m$^{1/2}$)	G_{IC}^{lam} (kJ/m^2)	K_{IC}^{lam} (MPa m$^{1/2}$)	K_{IC}^{lam} (MPa m$^{1/2}$)	K_{IC}^{lam} (MPa m$^{1/2}$)
Ref.	[12]	[24]	[22]	[19]	[20]	[11]	[21]
Material system	Woven flax/epoxy	Woven jute/epoxy	Fabric sisal/polyester	Fabric and short fiber sisal/PU	Fabric sisal/vinyl ester	Jute and hemp mat/polyester	Woven kenaf/polyester
Fiber content	V_f= 0.31–0.35	50 wt%	V_f=0.50–0.55	V_f≈ 0.30	V_f≈ 0.32	V_f≈ 0.41	No available
Toughness	(3–8.5) 7.2 (V_f≈ 0.33)	7.71	6.5	11.5 and 7	4.2–6	5.04 and 5.62	8.5

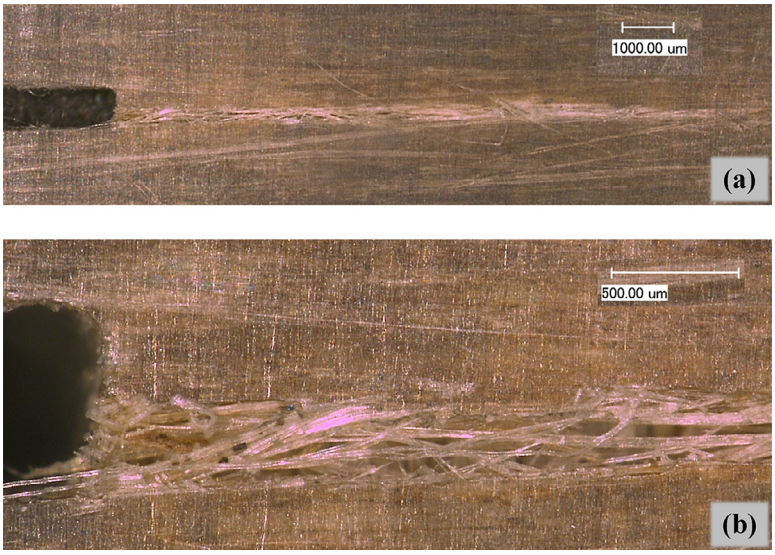

Fig. 7. Fracture path of cross-ply ECT specimen; (a) whole crack growth after failure, (b) fiber bridging.

fiber pull-out without a corresponding large energy absorption. This effect will cause fiber pull-out to share a smaller contribution to fracture toughness. There is no information in the literature about the fracture toughness of flax fibers; however, these might be some reasons why FFREC is offering lower TFT compared to engineered FRCs. The top view, Fig. 8(d), reveals the depth of the pulled-out fibers and the severity of this phenomenon.

4.3. Infrared thermography method

Subjecting six CT to tensile load and seven CC specimens to compression load, the translaminar fracture tests were conducted according to the method described above. Typical temperature variation fields measured using IRT associated with the crack propagation are presented in Fig. 9. The temperature increase observed during crack propagation is clearly higher for the CT specimens than for the CC ones: increasing of about 5 °C for CT and less than 2 °C for CC. This result confirms the usual conclusion that the fracture toughness of translaminar failure is higher in tension than in compression [28,30,33,35]. Moreover, the extent of warming over the coupon is larger for compression; this means the phenomenon of compressive failure creates a larger area of damage.

The corresponding load-displacement curves of CT and CC tests are plotted in Fig. 10(a) and (b), respectively. For all the CT and CC tests, the crack propagation started about at maximum load. The CT specimens experienced a progressive propagation of crack during the load drop. The two first CC tests, CC1 and CC2, had to be stopped at 6.5 mm of displacement due to a contact between the edges of the notch. Then the other CC tests were continued until 5.5 mm of displacement and the sample unloaded until diminishing of the load.

Finally, the intrinsic dissipation was evaluated using the IRT measure for CT (Fig. 10(c)) and CC specimens (Fig. 10(d)). For the CT specimens, the intrinsic dissipation is significant (value higher than 4×10^6 J/m^3) and concentrated at the crack edges. In Fig. 10(c), the edges of the sample are also seen due to the movement of the sample during the test. Evidently, the value of the intrinsic dissipation evaluated at the sample edges should not be considered. For the CC specimens, the intrinsic dissipation is relatively low (a value lower than 0.5×10^6 J/m^3), and the crack path is barely detectable. Moreover, due to the scale used in Fig. 10(d), some measured noises are visible. As will be explained in the two subsequent sections, according to the literature data for synthetic FRCs, G_{IC} in compression is lower than in tension. Therefore, knowing that the generated heat is proportional to G_{IC}, it is logical to obtain lower intrinsic dissipation for CC specimens than for CT specimens. However, for the authors, the obtained result for CC tests seems too low. Since IRT measures the temperature only at the surface, this might be due to the delamination (observed in compression testing of FFREC [56]) and possible buckling of the outer plies, which would hide a significant part of the created heat. Hence, it will not be possible to evaluate the real temperature inside the laminate.

4.4. Tension testing of CT specimens

Globally, CT specimens exhibit a brittle behavior with a relatively linear response up to almost the maximum load, which is followed by a sudden and then continuous force drop, indicating consistent crack growth and stiffness reduction, as shown in Fig. 10(a). These curves are very similar and are in good agreement with those reported in the literature for CT specimens of carbon/epoxy composites [28,31,32,35], which is as such an indication of the validity of the current tests. Therefore, they seem to have small enough damage zone to use the ASTM D5045 standard, which is developed for isotropic plastic materials, to evaluate the fracture toughness for comparison purposes. The fracture energy of the UD laminate (G_{IC}^{Ten}) was calculated using the same approach applied to ECT specimens, and the results are summarized in Table 6.

As shown in Fig. 9, for CT specimens, the damage zone is minimal; this was also observed by Pinho et al. [28] using C-Scan. The propagation of the crack is perceivable from the thermal image exposed in Fig. 9(a). As discussed above, considering the available values for β of

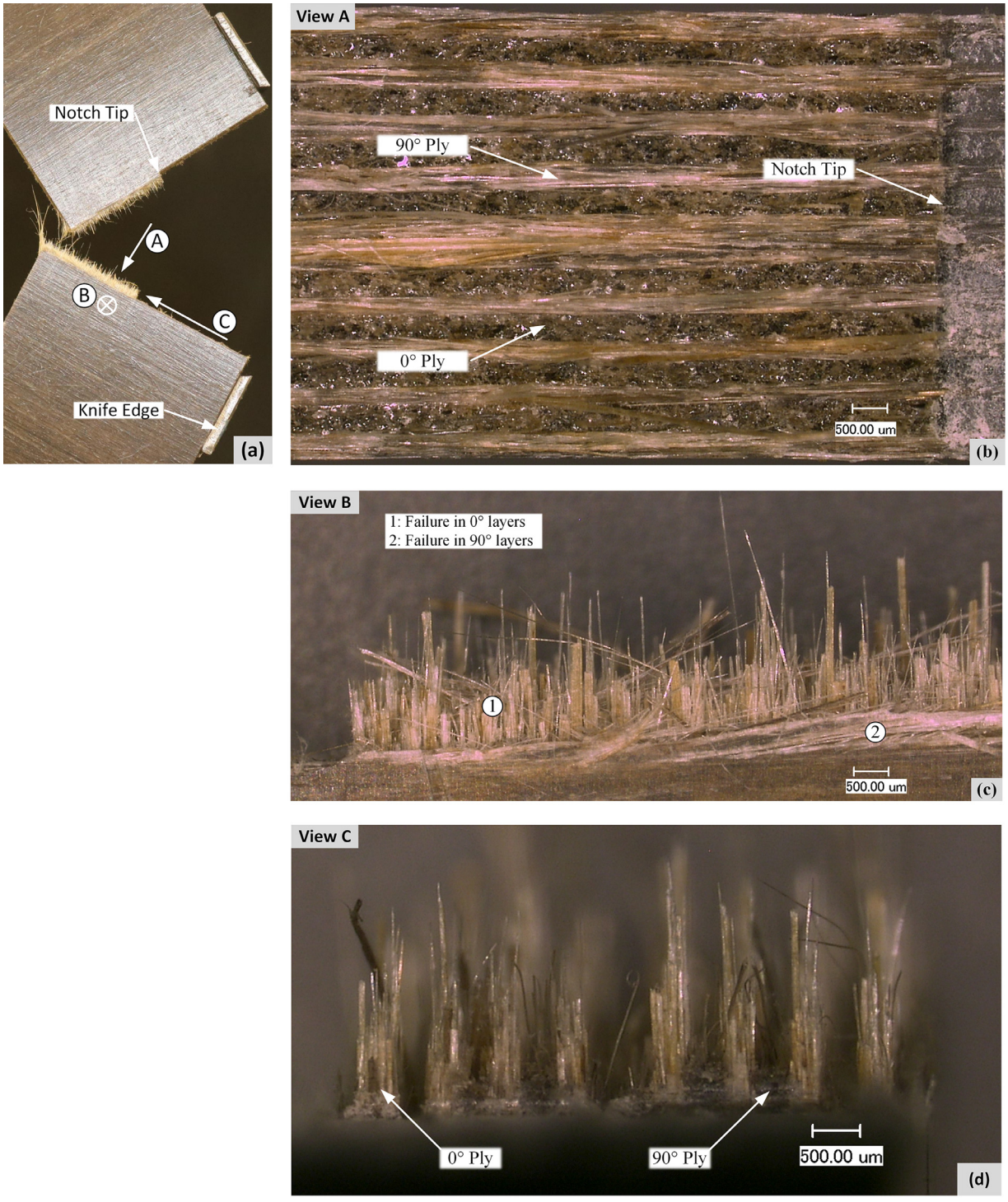

Fig. 8. Fracture surface of cross-ply ECT specimen; (a) definition of the viewing directions, (b) normal view to fracture surface, (c) normal view to specimen surface and (d) view parallel to the notch.

polymers in the literature, two cases were investigated; first assuming $\beta = 0.5$ and second, $\beta = 0.9$. Data treatment in the selected zones was performed according to the developed and validated methodology in [45,49]. The obtained fracture energy value is presented in Table 6.

It can be seen that the value of G_{IC}^{Ten} obtained by ASTM D5045, which was developed for isotropic plastic materials, is much (≈49%) higher than that determined by ASTM E1922, specially developed for FRCs. The later was particularly developed and validated based on synthetic FRCs, though, according to the standard, it is applicable to other types of FRPCs provided that the criteria are met. However, in this study, it was applied to NFRPCs, which have a more complicated microstructure and may behave differently. This is because NFs are composite by themselves that normally come in bundles containing technical fibers that are composed of helically arranged microfibrils as the main force carrying elements. Therefore, they exhibit more complex failure behavior with high variability in the material properties. The complex microstructure of the NFs will impose a complex fiber fracture leading to different mechanisms of energy absorption. Consequently, as a domi-

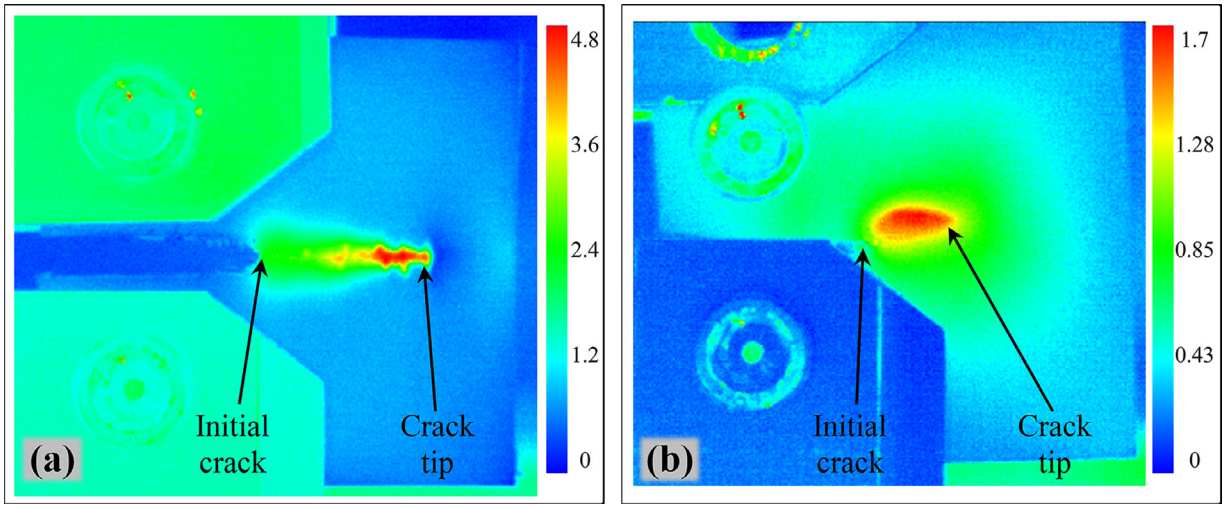

Fig. 9. Temperature variation field observed during the crack propagation of CT, (a) and CC, (b) specimens.

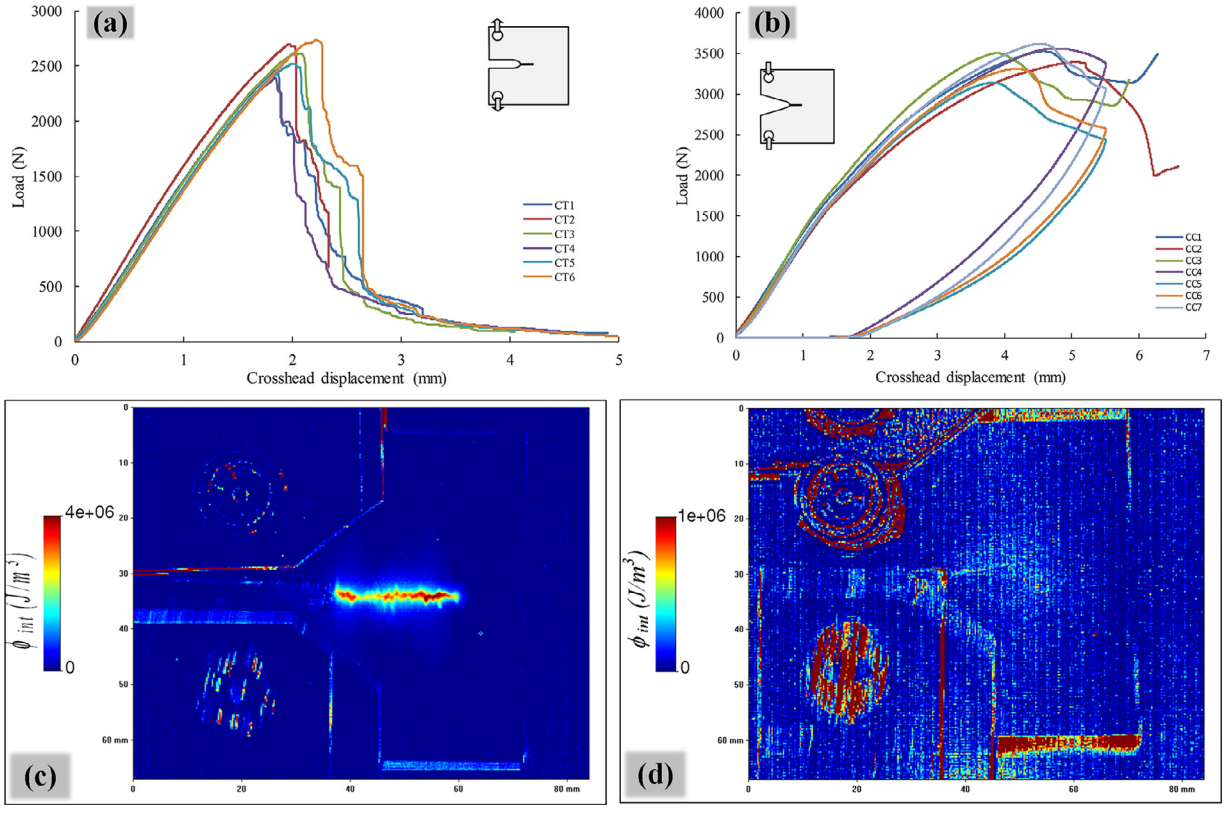

Fig. 10. Load–displacement curves for the CT (a) and CC (b) specimens, and intrinsic heat measured by IRT for the CT (c) and CC (d) specimens.

Table 6
Fracture toughness and fracture energy of UD-FFREC evaluated by IRT and standard methods

	IRT				ASTM standards			
	G_{IC}^{Ten} (kJ/m^2)		G_{IC}^{Comp} (kJ/m^2)		G_{IC}^{Ten} (kJ/m^2)	G_{IC}^{Ten} (kJ/m^2)	G_{IC}^{Comp} (kJ/m^2)	$G_{IC}^{Comp(Linear)}$ (kJ/m^2)
					E1922	D5045		
	$\beta = 0.50$	$\beta = 0.90$	$\beta = 0.50$	$\beta = 0.90$		Max Load		Max Linear
Mean	19.88	11.10	1.30	0.77	15.71	23.37	41.29	9.84
STD	2.68	1.49	0.119	0.066	1.23	2.28	3.56	0.39
COV (%)	13.48	13.42	9.15	8.57	7.82	9.76	8.62	4.00

nant failure mechanism, the complex fracture of NFs will influence the fracture toughness of the composite and may require a different determination method.

Nevertheless, there is no standard test method developed for testing NFRPCs and no literature data available to validate the results. Consequently, for the time being, G_{IC}^{Ten}determined by ASTM E1922 can be considered as the most reliable tensile TFT value for the understudy FFRECs. This value is placed between the values obtained by IFT analysis for $\beta = 0.90$ and $\beta = 0.50$by ±29% difference. Considering the high variability of material properties for NFs, these values could be considered consistent with that of the standard method. In general, even the data available for synthetic FRPCs are scattered, for instance, CT tests of a unique CFRP composite show more than 15% variation [30,35]. However, assuming the result of the standard method as the real value, it may be concluded that the realistic value of β for the understudy flax/epoxy is between the margins (0.50 and 0.90) used for analysis, or, technically speaking, the ratio of dissipative work converted into heat in this composite is between 50% and 90%. Considering that G_{IC} is an inverse linear function of β, this ratio for the composite can be calculated back from the result of the standard test ($\beta = 0.69$) and be used in the future calculation of the fracture energy, for instance in compressive failure mode, presented in the following section. Consequently, having a precise enough value for β, the employed method based on IRT can be confidently used to determine the fracture energy of the composites.

Naturally, the failure modes in CT specimens are the same occurring in ECT, as discussed in the previous section.

4.5. Compression testing of CC specimens

The load-displacement response of the CC tests (Fig. 10(b)) is more difficult to interpret. As can be observed, CC specimens exhibited complex, but similar behavior in compression loading. The similarity of the curves indicates a good reproducibility and the certainty of the data recorded for the composites under study. The composite displays a linear behavior up to a displacement of about 1.2 mm (1500 N of loading), where a clear slope reduction happens. After this point, a relatively linear response continues until a displacement of 3 mm followed by a nonlinear curve up to the maximum load. For all of the specimens, the visual signs of failure occurred at the maximum load, and upon reaching this point, the load slowly dropped until the test was stopped. The load-displacement response of these CC specimens is more or less analogous to that of carbon/epoxy CC specimens [28,30]; however, flax/epoxy composite demonstrates much higher nonlinearity. The ASTM D5045 standard was first employed to evaluate the fracture toughness in compression of the cross-ply laminate using the maximum load. Then, the fracture energy of the UD laminate in compression (G_{IC}^{Comp}) was calculated following the aforementioned approach used by Pinho et al. [28] for CC specimens and assuming that G_{IC}^{90} is equivalent in magnitude to the mode-II interlaminar fracture energy of the UD-FFREC, G_{IIC}^{delam}, which was evaluated in a separate study as $G_{IIC}^{delam} = 0.378$ kJ/m^2, the results are summarized in Table 6. However, the result is unreasonably higher compared to G_{IC}^{Ten}, whereas it is expected to be lower for compression testing [28,30,33,35]. This should be due to the nonlinearity that corresponds to some damages or plasticity in the sample and means that an important part of the dissipated energy is not due to the crack propagation but to other secondary damage phenomena. Therefore, the onset of damage must have happened much before reaching the maximum load point. Considering the low stiffness of flax fibers in compression and the poor fiber-matrix adhesion, this failure mode is a matrix-driven failure. Thus, it is expected that the isotropic epoxy matrix exhibits a linear behavior up to failure. Therefore, theoretically, the composite translaminar failure in compression should start in the endpoint of the first linear part, after which, by the development of other secondary material damages, the stiffness of the sample and the slope of the curve reduce. As a result, the load at this point is considered as the compressive translaminar failure load and is used to evaluate the $G_{IC}^{Comp}$of the composite, the result is presented in Table 6. The literature data for $G_{IC}^{Comp}$is very scattered, for instance, conducting 4-point bending tests, Laffan et al. [61] measured value of $G_{IC}^{Comp} = 25.9$ kJ/m^2 for IM7/8552 CFRP, while Catalanotti et al. [30] reported $G_{IC}^{Comp} = 47.5$ kJ/m^2 for the same material system and Pinho et al. [28] published $G_{IC}^{Comp} = 79.9$ kJ/m^2 for another CFRP, both using CC specimens. Therefore, the value in this range can be a good representative of the fracture energy of the composite. Nevertheless, the complex microstructure of the NF composite and, consequently, its complex behavior increases the difficulty of recognizing the precise failure point and needs deeper analysis.

Fig. 9 shows that CC specimens experience much broader damage zone compared to CT specimens, also observed by Pinho et al. [28]. However, the onset of failure and propagation of the crack couldn't be recognized in the thermal images and the experimental heat source fields.

In a similar approach to CT tests, assuming $\beta = 0.50$ and $\beta = 0.90$ the data were processed to determine the translaminar fracture energy in compression (G_{IC}^{Comp}), and the obtained values are given in Table 6. As expected, the values are lower than those for CT tests, though they are obviously too low, indicating that the IRT methodology is underestimating the fracture energy in compression for these composites. There is no available literature data for $G_{IC}^{Comp}$to be compared with the obtained values; however, the proportion of the G_{IC}^{Ten} to G_{IC}^{Comp} for other composites evidently shows that these the measured values by IFT do not represent the$G_{IC}^{Comp}$of the composite. Considering the presence of complex failure modes in CC specimens, which is more complicated for NF composites, it is not trivial to perform a root-cause-analysis for this issue; however, some hypotheses can be made. A previous study shows that the UD-FFREC experiences delamination damage in compression failure [56]; this may be the case for the cross-ply CC specimen. Therefore, the surface layer might have been delaminated before a translaminar failure occurs and then buckled in the out-of-plane direction so that the generated heat in the surface ply is not associated with a translaminar failure and could be the result of other failure modes, like buckling, producing much less heat. It could also be related to the microstructure of the flax fibers so that, under compression loading, their internal structure collapses, with the fibers being compressed in themselves to generate reversible energy, rather than failing to produce thermal energy. Finally, the poor fiber-matrix adhesion could make the fibers ineffective in carrying the compression load; thus, the fracture energy could be mostly related to matrix failure in compression. This hypothesis is supported by Mode-II interlaminar fracture energy of UD-FFREC, $G_{IIC}^{delam} = 0.378$ kJ/m^2, measured in another study [58], as their failure modes are similar, and the fracture energy values are close.

In summary, using IRT and cross-ply laminates, valid values cannot be determined for $G_{IC}^{Comp}$of the UD-FFRECs. However, assuming that the failure starts at the end of the first linear part of the load-displacement curve and using the ASTM D5045 standard, a reasonable value can be achieved for $G_{IC}^{Comp}$of the UD-FFRECs.

5. Conclusions

This study has investigated the fracture behavior and evaluated the fracture toughness parameters of the UD-FFRECs under quasi-static tensile and compressive loads. The existing ASTM E1922 standard test method was employed to examine the fracture toughness of ECT specimens in tension, and an already developed methodology based on IRT, as well as ASTM D5045, were applied to study the fracture energy in tension and compression respectively using CT and CC specimens. Afterward, combining the micrographs and the load-NMOD curves, the fracture behavior and the fracture mechanisms of the composite were studied.

Applying the ASTM E1922 standard test method to determine the tensile fracture toughness using UD laminates was impossible, and the

self-similar translaminar crack growth of concern was not exhibited. A cross-ply laminate was instead used to evaluate the fracture toughness of the laminate and extract that of UD composite following an approach that was already used and proved valid in some earlier studies. Although there are no published fracture property data for these composites for comparison, the obtained values (G_{IC} = 15.71 kJ/m^2 and K_{IC} = 14.27 MPa m$^{1/2}$) fit very well in the range of those of the similar NFPCs available in the literature.

Experimental tests using IRT were conducted, and employing the developed program, the data were treated to determine the fracture toughness of the composite in tensile and compressive loadings using CT and CC cross-ply composite specimens, respectively. An assumption of $\beta = 0.5$ and $\beta = 0.9$ was made for the Taylor–Quinney coefficient based on the existing values for similar materials. Compared to the standard test results, CT specimens demonstrated proper adequacy for this purpose; however, the results of CC tests were too low and thus unsatisfactory. Employing this methodology to CT tests, the values of $G_{IC}^{Ten} = 19.88$ and 11.1 kJ/m^2, respectively for $\beta = 0.5$ and $\beta = 0.9$, were obtained. The results of IRT are consistent with and are covering those of the ASTM E1922, showing that the real value of β is between the two assumed values. Therefore, the application of the IRT method for evaluating tensile translaminar fracture energy of UD-flax/epoxy composites using CT tests is validated; however, the accuracy of IRT for determining the compressive translaminar fracture energy using CC specimens is not proved. Instead, for CC tests it was concluded that using the maximum load of the initial linear load-displacement curve as the failure load and ASTM D5045 standard leads to a reasonable compressive fracture energy $G_{IC}^{Comp} = 9.84$ kJ/m^2. The fractography study reveals that the primary mechanisms activated in translaminar failure are fiber pull-out, fiber breakage, and fiber-matrix debonding. To conclude, a view of the translaminar fracture behavior of the UD-FFRECs has been drawn, and the translaminar fracture toughness parameters in the fiber direction and under tensile and compressive loadings are determined. These values are the most reliable data ever obtained to be used in engineering design and numerical simulation studies.

Declaration of Competing Interest

The authors declare that they have no known competing financial interests or personal relationships that could have appeared to influence the work reported in this paper.

CRediT authorship contribution statement

Yousef Saadati: Conceptualization, Investigation, Formal analysis, Data curation, Validation, Writing - original draft. **Gilbert Lebrun:** Conceptualization, Supervision, Writing - review & editing, Funding acquisition. **Christophe Bouvet:** Investigation, Methodology, Software, Formal analysis, Writing - review & editing. **Jean-François Chatelain:** Conceptualization, Supervision, Writing - review & editing, Funding acquisition. **Yves Beauchamp:** Conceptualization, Supervision, Writing - review & editing, Funding acquisition.

Acknowledgments

The authors sincerely thank Mr. Daniel Poirier and his colleagues from CDCQ (Centre de développement des composites du Québec), for molding the composite plates, as well as Serge Plamondon and Claude-Daniel Legault who provided technical assistance that greatly assisted us in this research. This work was supported by the Natural Sciences and Engineering Research Council of Canada (NSERC) [grant number RGPIN-2017-04305].

Data availability

The raw/processed data required to reproduce these findings cannot be shared at this time as the data also forms part of an ongoing study.

References

[1] T.G. Yashas Gowda, M.R. Sanjay, K. Subrahmanya Bhat, P. Madhu, P. Senthamaraikannan, B. Yogesha, Polymer matrix-natural fiber composites: an overview, Cogent Eng. 5 (2018) 1446667.
[2] M. Fuqua, S. Huo, C. Ulven, Natural fiber reinforced composites, Polym. Rev. 52 (2012) 259–320.
[3] M. Ramesh, K. Palanikumar, K. Reddy, Plant fibre based bio-composites: sustainable and renewable green materials, Renew. Sustain. Energy Rev. 79 (2017) 558–584.
[4] D.U. Shah, P.J. Schubel, M.J. Clifford, Can flax replace E-glass in structural composites? A small wind turbine blade case study, Compos. B: Eng. 52 (2013) 172–181.
[5] A. Moudood, A. Rahman, A. Öchsner, M. Islam, G. Francucci, Flax fiber and its composites: an overview of water and moisture absorption impact on their performance, J. Reinforc. Plast. Compos. 38 (2018) 323–339.
[6] L. Yan, N. Chouw, K. Jayaraman, Flax fibre and its composites – a review, Compos. B: Eng. 56 (2014) 296–317.
[7] S. Goutianos, T. Peijs, The optimisation of flax fibre yarns for the development of high-performance natural fibre composites, Adv. Compos. Lett. 12 (2003) 237–241.
[8] S. Goutianos, T. Peijs, B. Nystrom, M. Skrifvars, Development of flax fibre based textile reinforcements for composite applications, Appl. Compos. Mater. 13 (2006) 199–215.
[9] H.M. Khanlou, P. Woodfield, J. Summerscales, G. Francucci, B. King, S. Talebian, et al., Estimation of mechanical property degradation of poly(lactic acid) and flax fibre reinforced poly(lactic acid) bio-composites during thermal processing, Measurement 116 (2018) 367–372.
[10] S. Haldar, M. Herráez, F. Naya, C. González, C.S. Lopes, Relations between intralaminar micromechanisms and translaminar fracture behavior of unidirectional FRP supported by experimental micromechanics, Compos. B: Eng. 174 (2019) 107000.
[11] M. Hughes, C. Hill, J. Hague, The fracture toughness of bast fibre reinforced polyester composites Part 1 evaluation and analysis, J. Mater. Sci. 37 (2002) 4669–4676.
[12] Q. Liu, M. Hughes, The fracture behaviour and toughness of woven flax fibre reinforced epoxy composites, Compos. A: Appl. Sci. Manuf. 39 (2008) 1644–1652.
[13] B.G. Falzon, P. Apruzzese, Numerical analysis of intralaminar failure mechanisms in composite structures. Part I: FE implementation, Compos. Struct. 93 (2011) 1039–1046.
[14] R. El-Hajjar, R. Haj-Ali, Mode-I fracture toughness testing of thick section FRP composites using the ESE(T) specimen, Eng. Fract. Mech. 72 (2005) 631–643.
[15] A. Faggiani, B. Falzon, Predicting low-velocity impact damage on a stiffened composite panel, Compos. A: Appl. Sci. Manuf. 41 (2010) 737–749.
[16] H.A. Israr, S. Rivallant, C. Bouvet, J.J. Barrau, Finite element simulation of 0˚/90˚CFRP laminated plates subjected to crushing using a free-face-crushing concept, Compos. A: Appl. Sci. Manuf. 62 (2014) 16–25.
[17] S. Jose, R.R. Kumar, M. Jana, G.V. Rao, Intralaminar fracture toughness of a cross–ply laminate and its constituent sub-laminates, Compos. Sci. Technol. 61 (2001) 1115–1122.
[18] M.J. Laffan, S. Pinho, P. Robinson, A. McMillan, Translaminar fracture toughness testing of composites: a review, Polym. Test. 31 (2012) 481–489.
[19] R.V. Silva, D. Spinelli, W.W. Bose Filho, S. Claro Neto, G.O. Chierice, J.R. Tarpani, Fracture toughness of natural fibers/castor oil polyurethane composites, Compos. Sci. Technol. 66 (2006) 1328–1335.
[20] Y. Li, Y-W Mai, L. Ye, Effects of fibre surface treatment on fracture-mechanical properties of sisal-fibre composites, Compos. Interfaces 12 (2005) 141–163.
[21] A.E. Ismail, S.H. Masran, S. Jamian, K.A. Kamarudin, M.K. Mohd Nor, N.H.M. Nor, et al., Fracture toughness of woven kenaf fibre reinforced composites, IOP Conf. Ser.: Mater. Sci. Eng. 160 (2016) 012020.
[22] C. Chizyuka, Effects of hydrothermal ageing on the fracture damage of sisal fibre reinforced polyester composites, Zambian Eng. 46 (2013) 11–19.
[23] B.M. G, T.N. Vijaykumar, D.B. K N, Jmsse, Optimization of notch parameter on fracture toughness of natural fiber reinforced composites using taguchi method, J. Mater. Sci. Surf. Eng. 3 (2015) 244–248.
[24] K.P. Ashik, R.S. Sharma, N. Raghavendra, Evaluation of tensile, modal and fracture properties of jute/epoxy natural composites with addition of silicon di oxide as filler material, Mater. Today: Proc. 4 (2017) 9586–9591.
[25] ASTM, Standard Test Method for Translaminar Fracture Toughness of Laminated and Pultruded Polymer Matrix Composite Materials, ASTM International, West Conshohocken, PA, 2015.
[26] J. Underwood, M. Kortschot, W. Lloyd, H. Eidinoff, D. Wilson, N. Ashbaugh, Translaminar fracture toughness test methods and results from interlaboratory tests of carbon/epoxy laminates, Fract. Mech. 1256 (1995) 486–508 26th VolumeASTM STP.
[27] R. Piascik, J. Newman, J. Underwood, The extended compact tension specimen, Fatigue Fract. Eng. Mater. Struct. 20 (1997) 559–563.
[28] S.T. Pinho, P. Robinson, L. Iannucci, Fracture toughness of the tensile and compressive fibre failure modes in laminated composites, Compos. Sci. Technol. 66 (2006) 2069–2079.
[29] L.W.H. Leonard, K.J. Wong, K.O. Low, B.F. Yousif, Fracture behaviour of glass fibre-reinforced polyester composite, Proc. Inst. Mech. Eng. L: J. Mater.: Des. Appl. 223 (2009) 83–89.
[30] G. Catalanotti, P.P. Camanho, J. Xavier, C.G. Dávila, A.T. Marques, Measurement of resistance curves in the longitudinal failure of composites using digital image correlation, Compos. Sci. Technol. 70 (2010) 1986–1993.
[31] M.J. Laffan, S.T. Pinho, P. Robinson, L. Iannucci, Measurement of the in situ ply fracture toughness associated with mode I fibre tensile failure in FRP. Part I: data reduction, Compos. Sci. Technol. 70 (2010) 606–613.

[32] M.J. Laffan, S.T. Pinho, P. Robinson, L. Iannucci, Measurement of the in situ ply fracture toughness associated with mode I fibre tensile failure in FRP. Part II: size and lay-up effects, Compos. Sci. Technol. 70 (2010) 614–621.
[33] H. Liu, B. Falzon, G. Catalanotti, W. Tan, An experimental method to determine the intralaminar fracture toughness of high-strength carbon-fibre reinforced composite aerostructures, Aeronaut. J. 122 (2018) 1352–1370.
[34] S. Pinho, P. Robinson, L. Iannucci, Developing a four point bend specimen to measure the mode I intralaminar fracture toughness of unidirectional laminated composites, Compos. Sci. Technol. 69 (2009) 1303–1309.
[35] M.J. Laffan, S.T. Pinho, P. Robinson, A.J. McMillan, Translaminar fracture toughness: the critical notch tip radius of 0° plies in CFRP, Compos. Sci. Technol. 72 (2011) 97–102.
[36] M. Laffan, S. Pinho, P. Robinson, L. Iannucci, Fracture toughness measurement for mode i fibre tensile failure in FRP, in: Proceedings of the International Conference on Composite Materials, 2009.
[37] R.F. Teixeira, S.T. Pinho, P. Robinson, Thickness-dependence of the translaminar fracture toughness: experimental study using thin-ply composites, Compos. A: Appl. Sci. Manuf. 90 (2016) 33–44.
[38] M.V. Donadon, B.G. Falzon, L. Iannucci, J.M. Hodgkinson, Intralaminar toughness characterisation of unbalanced hybrid plain weave laminates, Compos. A: Appl. Sci. Manuf. 38 (2007) 1597–1611.
[39] C. Soutis, P. Curtis, A method for predicting the fracture toughness of CFRP laminates failing by fibre microbuckling, Compos. A: Appl. Sci. Manuf. 31 (2000) 733–740.
[40] R. Gutkin, S.T. Pinho, P. Robinson, P.T. Curtis, On the transition from shear-driven fibre compressive failure to fibre kinking in notched CFRP laminates under longitudinal compression, Compos. Sci. Technol. 70 (2010) 1223–1231.
[41] S. Dumoulin, H. Louche, O.S. Hopperstad, T. Børvik, Heat sources, energy storage and dissipation in high-strength steels: experiments and modelling, Eur. J. Mech. – A/Solids 29 (2010) 461–474.
[42] B. Wattrisse, J-M Muracciole, A. Chrysochoos, Thermomechanical effects accompanying the localized necking of semi-crystalline polymers, Int. J. Therm. Sci. 41 (2002) 422–427.
[43] M. Naderi, A. Kahirdeh, M.M. Khonsari, Dissipated thermal energy and damage evolution of Glass/Epoxy using infrared thermography and acoustic emission, Compos. B: Eng. 43 (2012) 1613–1620.
[44] T. Lisle, C. Bouvet, M-L Pastor, T. Rouault, P. Margueres, Damage of woven composite under tensile and shear stress using infrared thermography and micrographic cuts, J. Mater. Sci. 50 (2015) 6154–6170.
[45] T. Lisle, C. Bouvet, M.L. Pastor, P. Margueres, R. Prieto Corral, Damage analysis and fracture toughness evaluation in a thin woven composite laminate under static tension using infrared thermography, Compos. A: Appl. Sci. Manuf. 53 (2013) 75–87.
[46] L.B. Freund, JW. Hutchinson, High strain-rate crack growth in rate-dependent plastic solids, J. Mech. Phys. Solids 33 (1985) 169–191.
[47] R. Kapoor, S. Nemat-Nasser, Determination of temperature rise during high strain rate deformation, Mech. Mater. 27 (1998) 1–12.
[48] Z. Li, J. Lambros, Strain rate effects on the thermomechanical behavior of polymers, Int. J. Solids Struct. 38 (2001) 3549–3562.
[49] T. Lisle, C. Bouvet, N. Hongkarnjanakul, M-L Pastor, S. Rivallant, P. Margueres, Measure of fracture toughness of compressive fiber failure in composite structures using infrared thermography, Compos. Sci. Technol. 112 (2015) 22–33.
[50] T. Lisle, N. Hongkarnjanakul, C. Bouvet, M-L Pastor, P. Margueres, S. Rivallant, Measure of fracture toughness in composite structures using infrared thermography, in: Proceedings of the ECCM16 – Sixteenth European Conference on Composite Materials, Seville, Spain, 2014.
[51] N. Hongkarnjanakul, C. Bouvet, S. Rivallant, Validation of low velocity impact modelling on different stacking sequences of CFRP laminates and influence of fibre failure, Compos. Struct. 106 (2013) 549–559.
[52] J.D. Pujols Gonzalez, C. Bouvet, B. Vieille, Translaminar cracking modelling in woven ply composite laminates at high temperature, in: Proceedings of the ECCM19 – Nineteenth European Conference on Composite Materials, Nantes, France, 2020.
[53] F. Hou, S. Hong, Characterization of R-curve behavior of translaminar crack growth in cross-ply composite laminates using digital image correlation, Eng. Fract. Mech. 117 (2014) 51–70.
[54] P. Paris, G. Sih, Stress analysis of cracks, in: Fracture Toughness Testing and its Applications Chicago: ASTM-STP 381, 1965, pp. 30–83.
[55] S.T. Lin, Z. Feng, R.E. Rowlands, Thermoelastic determination of stress intensity factors in orthotropic composites using the J-integral, Eng. Fract. Mech. 56 (1997) 579–592.
[56] Y. Saadati, G. Lebrun, J.-F. Chatelain, Y. Beauchamp, Experimental investigation of failure mechanisms and evaluation of physical/mechanical properties of unidirectional flax–epoxy composites, J. Compos. Mater. (2020) 0021998320902243.
[57] M.W. Hyer, SR. White, Stress Analysis of Fiber-Reinforced Composite Materials, DEStech Publications, Inc, 2009.
[58] Y. Saadati, J-F Chatelain, G. Lebrun, Y. Beauchamp, P. Bocher, N. Vanderesse, A study of the interlaminar fracture toughness of unidirectional flax/epoxy composites, J. Compos. Sci. 4 (2020) 66.
[59] D.K. Rajak, D.D. Pagar, P.L. Menezes, E. Linul, Fiber-reinforced polymer composites: manufacturing, properties, and applications, Polymers 11 (2019) 1667.
[60] M. Habibi, G. Lebrun, L. Laperrière, Experimental characterization of short flax fiber mat composites: tensile and flexural properties and damage analysis using acoustic emission, J. Mater. Sci. 52 (2017) 6567–6580.
[61] M. Laffan, S. Pinho, P. Robinson, L. Iannucci, A. McMillan, Measurement of the fracture toughness associated with the longitudinal fibre compressive failure mode of laminated composites, Compos. A: Appl. Sci. Manuf. 43 (2012) 1930–1938.